Supplementary Information

Tuning the thermoelectric properties of metallo-porphyrins

Qusiy H. Al-Galiby[†a,b], Hatef Sadeghi[†a], Laith A. Algharagholy[†a,c,d] , Iain Grace[†a] and *Colin Lambert[†a]

[a]Quantum Technology Centre Department of Physics, Lancaster University, Lancaster LA1 4YB, UK

[b]Department of Physics Al Qadisiyah University, Al Qadisiyah, 58002, IRAQ

[c]College of Basic Education, Sumer University, Al-Refayee, Thi-Qar, 64001, IRAQ

[d]College of Computer Science and Mathematics, Al-Qadisiyah University, Al-Qadisiyah, Diwaniyah, 58002, IRAQ.

[†]Authors contributed.

*Corresponding author: c.lambert@lancaster.ac.uk

Charge transfer between the metal atom and porphyrin host.

Table S1: Spin-DFT-PBI calculation of the number of spin up and spin down electrons on each metal atom χ , along with the number ΔN of electrons lost by the metal atoms to the porphyrin host.

Atom	Spin up	Spin down	Total No. of electrons	ΔN
Co	4.70	3.41	8.12	0.88
Cu	5.37	4.85	10.2	0.77
Fe	4.64	2.02	6.66	1.34
Mn	5.23	0.67	5.90	1.1
Zn	4.58	4.58	9.16	0.84
Ni	4.62	4.62	9.25	0.75

Plots of frontier orbitals and spin-dependent transmission coefficients.

The spin dependent transport calculations show similar behaviour for T(E) for both up spin and down spin close to the Fermi energy (0eV) in all P- χ molecules. However, at higher energies, there can be large differences between the two. For example, in the case of P-Fe (**Fig S2**), at an energy value of $E-E_F$ ~2eV the transmission resonances differ. The spin up transmission curve shows a clear antiresonance, and this resonance has the shape of a Fano resonance, while the down spin shows a normal Breit-Wigner resonance. This difference can be explained by the nature of the LUMO orbitals which for the spin down are all delocalized along the molecular backbone but for the spin up, the LUMO+1 and LUMO+2 orbitals are clearly localized on the central unit of the molecule.

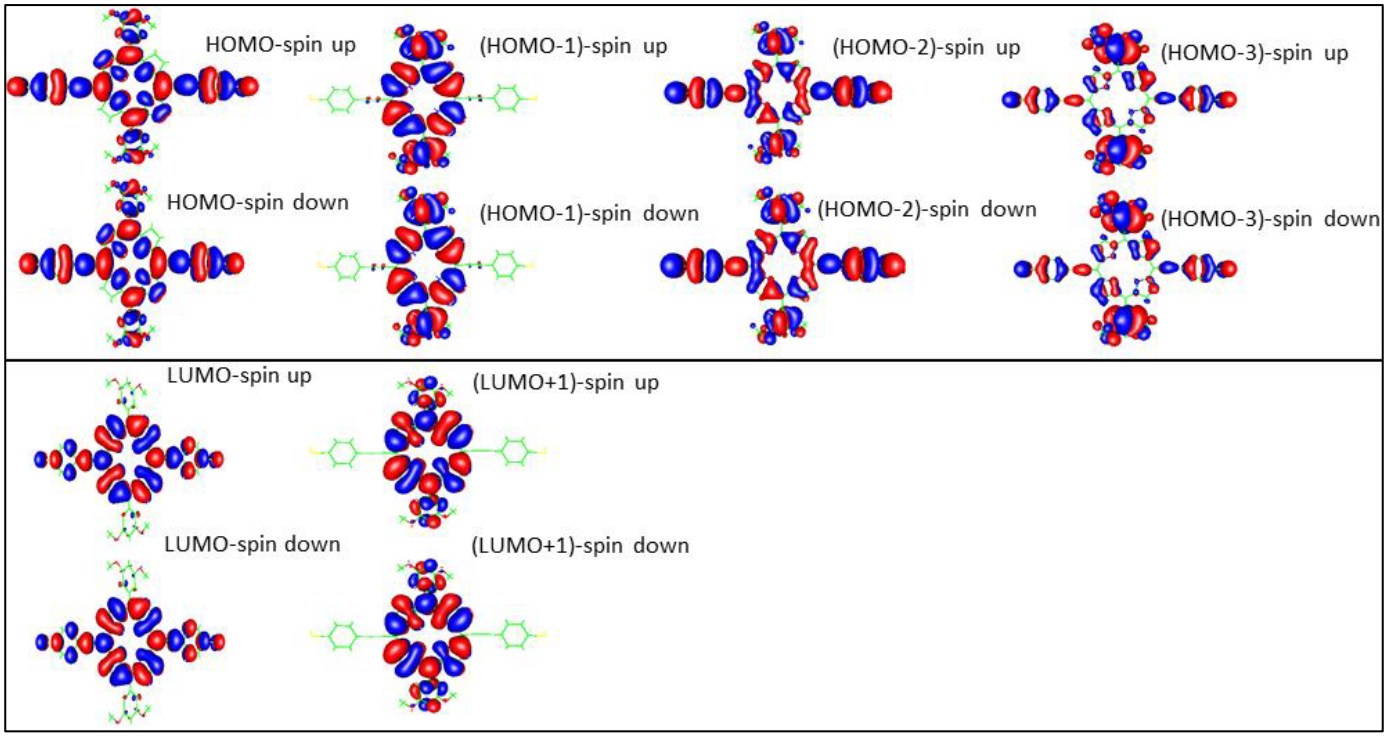

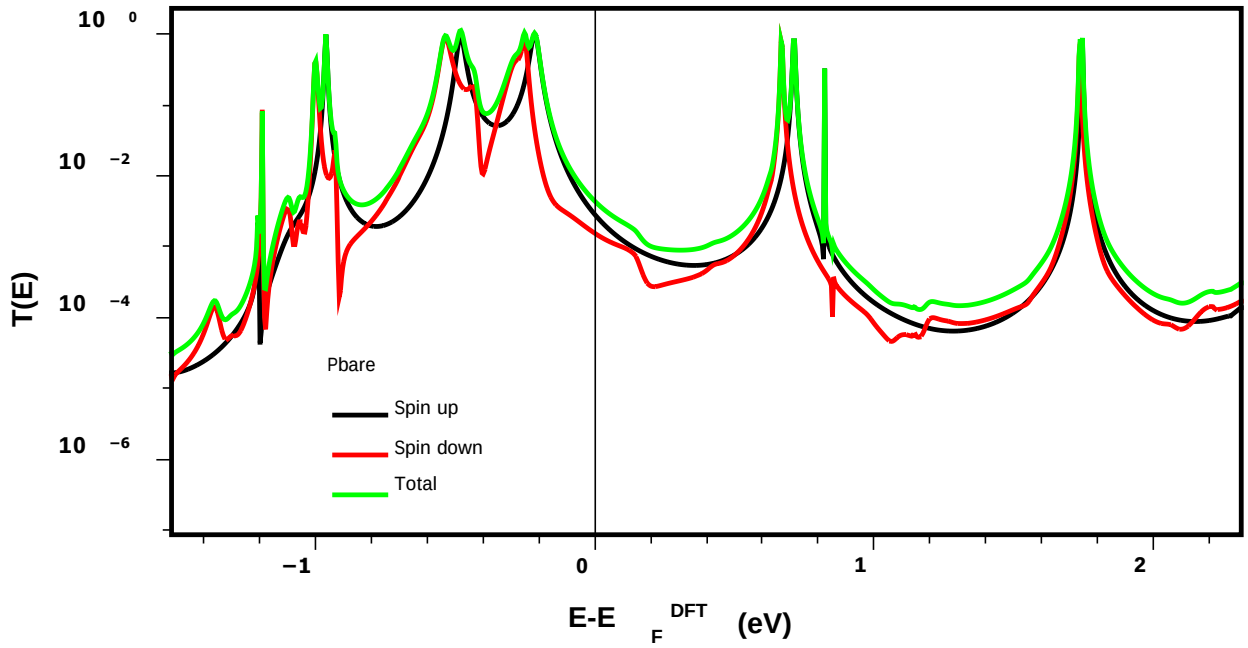

Figure S1: Frontier molecular orbitals of the P-bare obtained using the spin- dependent DFT. Red corresponds to positive and blue to negative regions of the wave functions. Below each plot of molecular orbitals, we present the spin-dependent and total transmission coefficients as a function of energy.

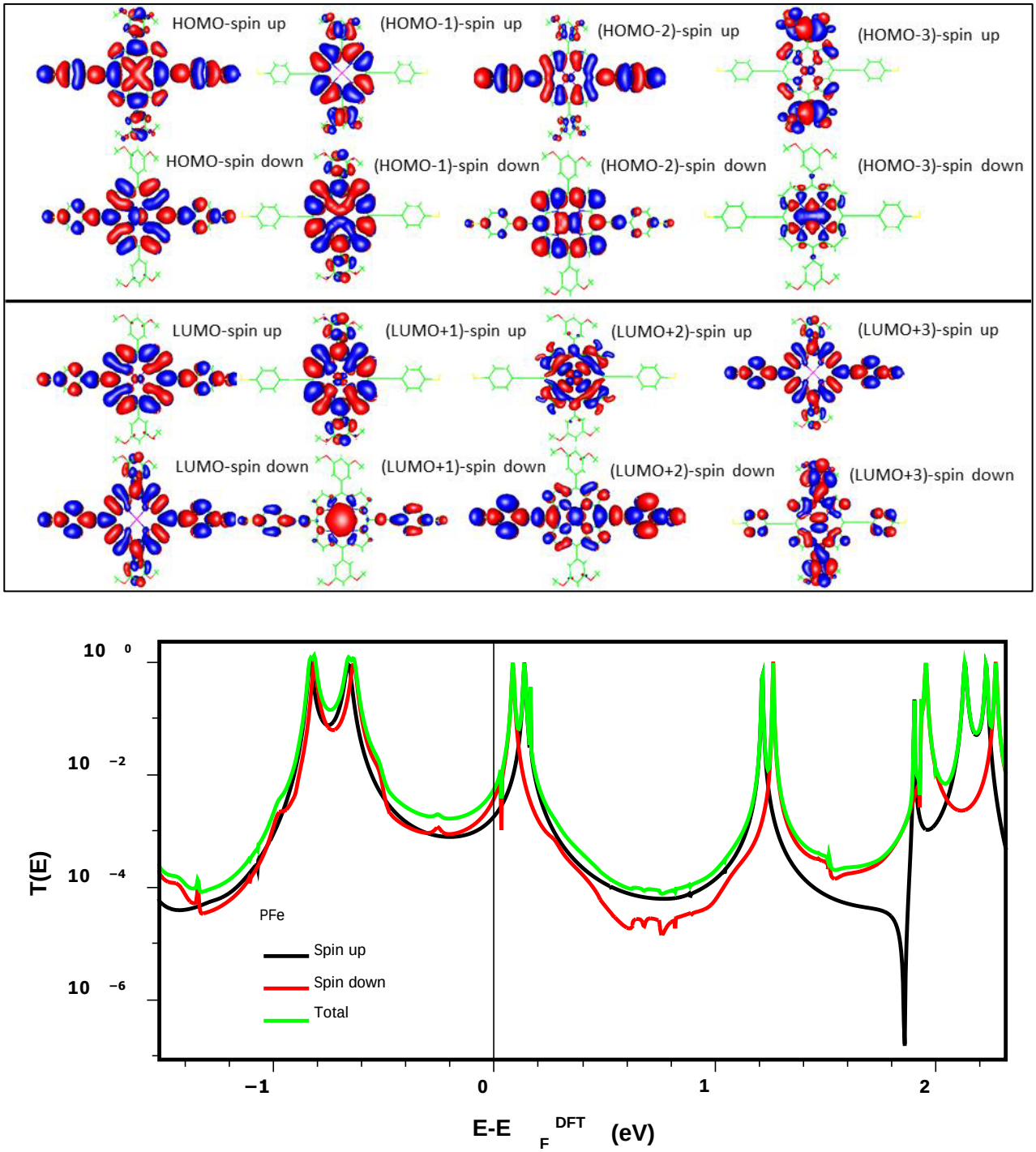

Figure S2: Frontier molecular orbitals of the PFe obtained using the spin- dependent DFT. Red corresponds to positive and blue to negative regions of the wave functions. Below each plot of molecular orbitals, we present the spin-dependent and total transmission coefficients as a function of energy.

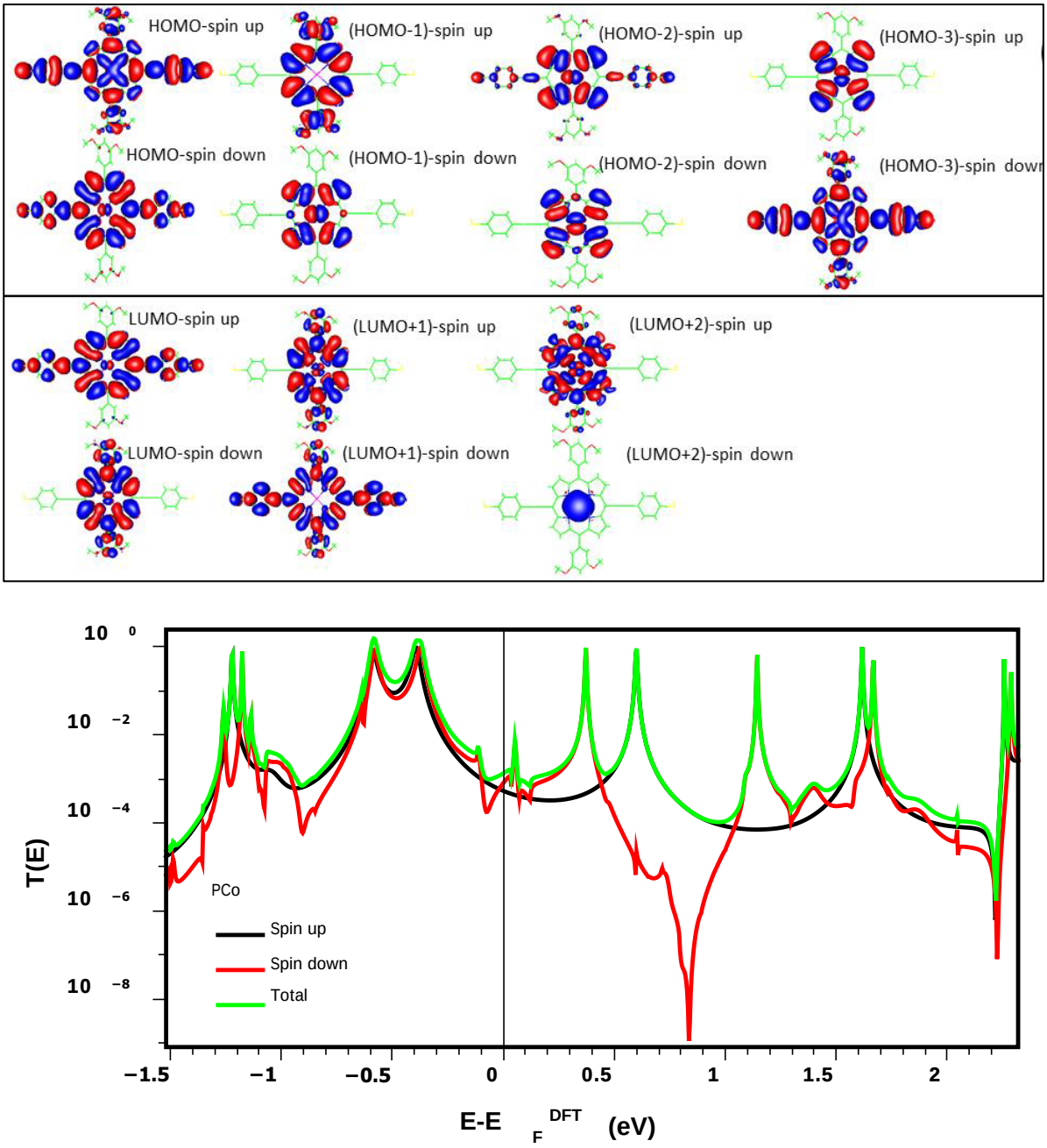

Figure S3: Frontier molecular orbitals of the PCo obtained using the spin- dependent DFT. Red corresponds to positive and blue to negative regions of the wave functions. Below each plot of molecular orbitals, we present the spin-dependent and total transmission coefficients as a function of energy.

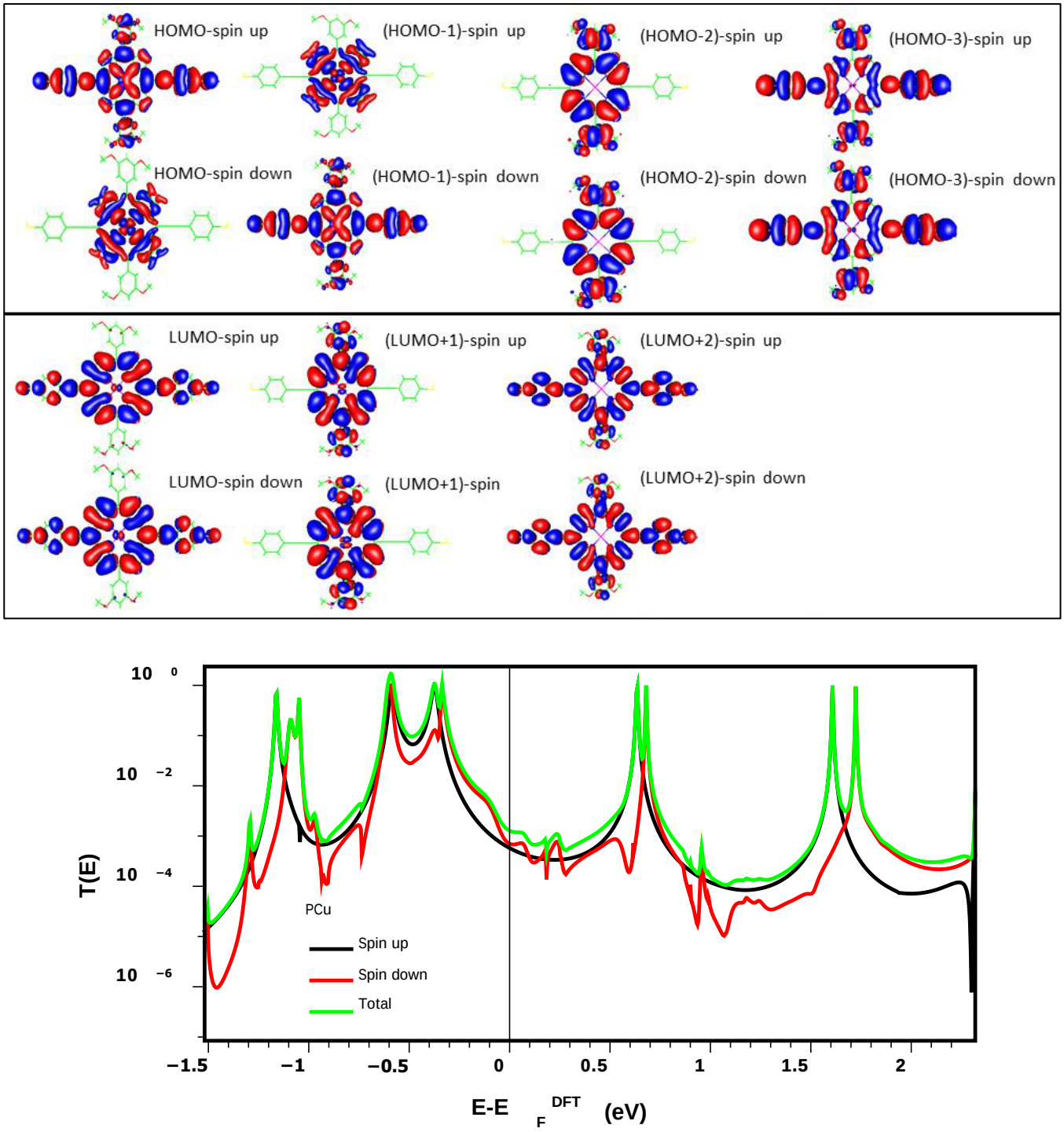

Figure S4: Frontier molecular orbitals of the PCu obtained using the spin- dependent DFT. Red corresponds to positive and blue to negative regions of the wave functions. Below each plot of molecular orbitals, we present the spin-dependent and total transmission coefficients as a function of energy.

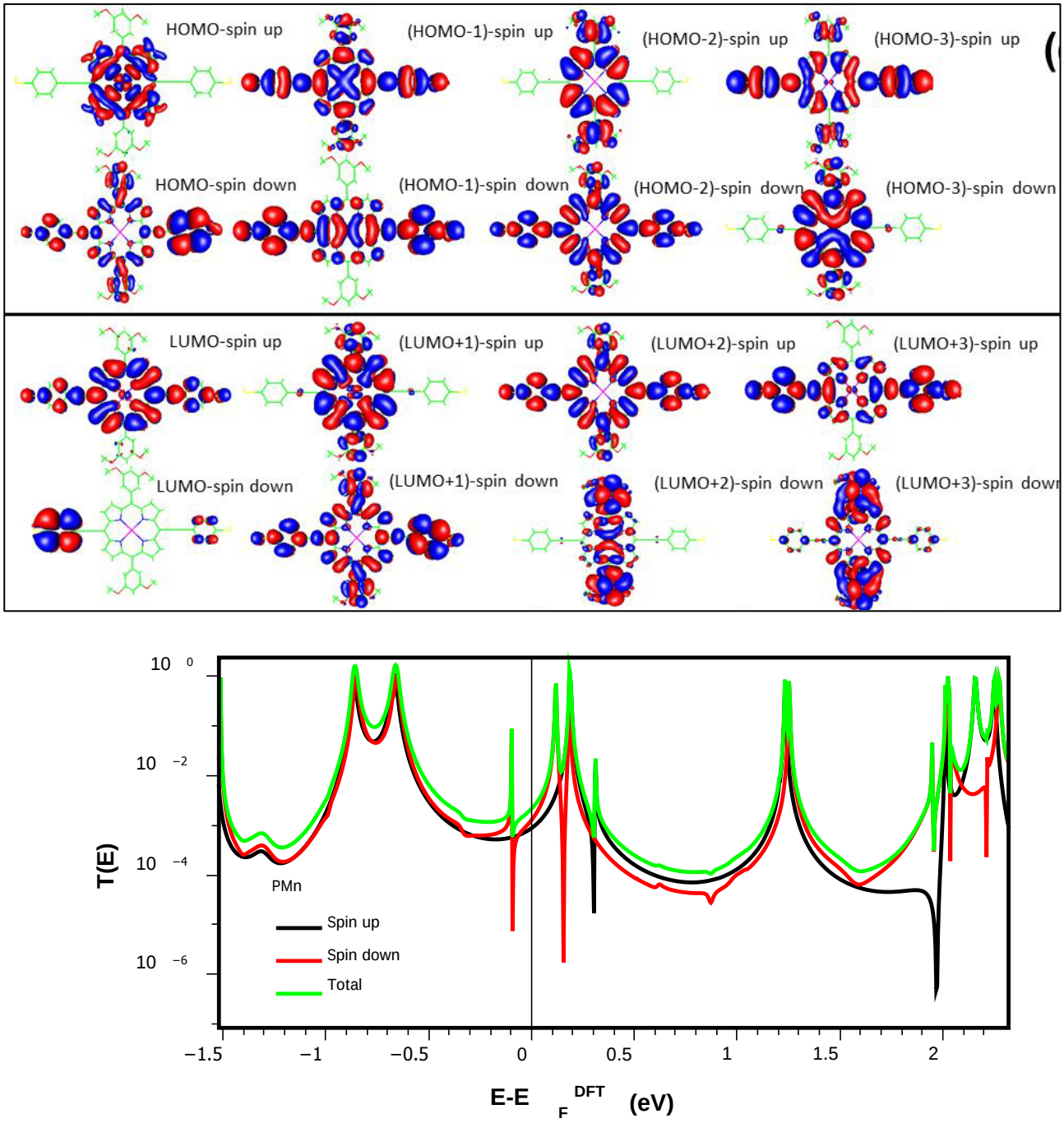

Figure S5: Frontier molecular orbitals of the PMn obtained using the spin- dependent DFT. Red corresponds to positive and blue to negative regions of the wave functions. Below each plot of molecular orbitals, we present the spin-dependent and total transmission coefficients as a function of energy.

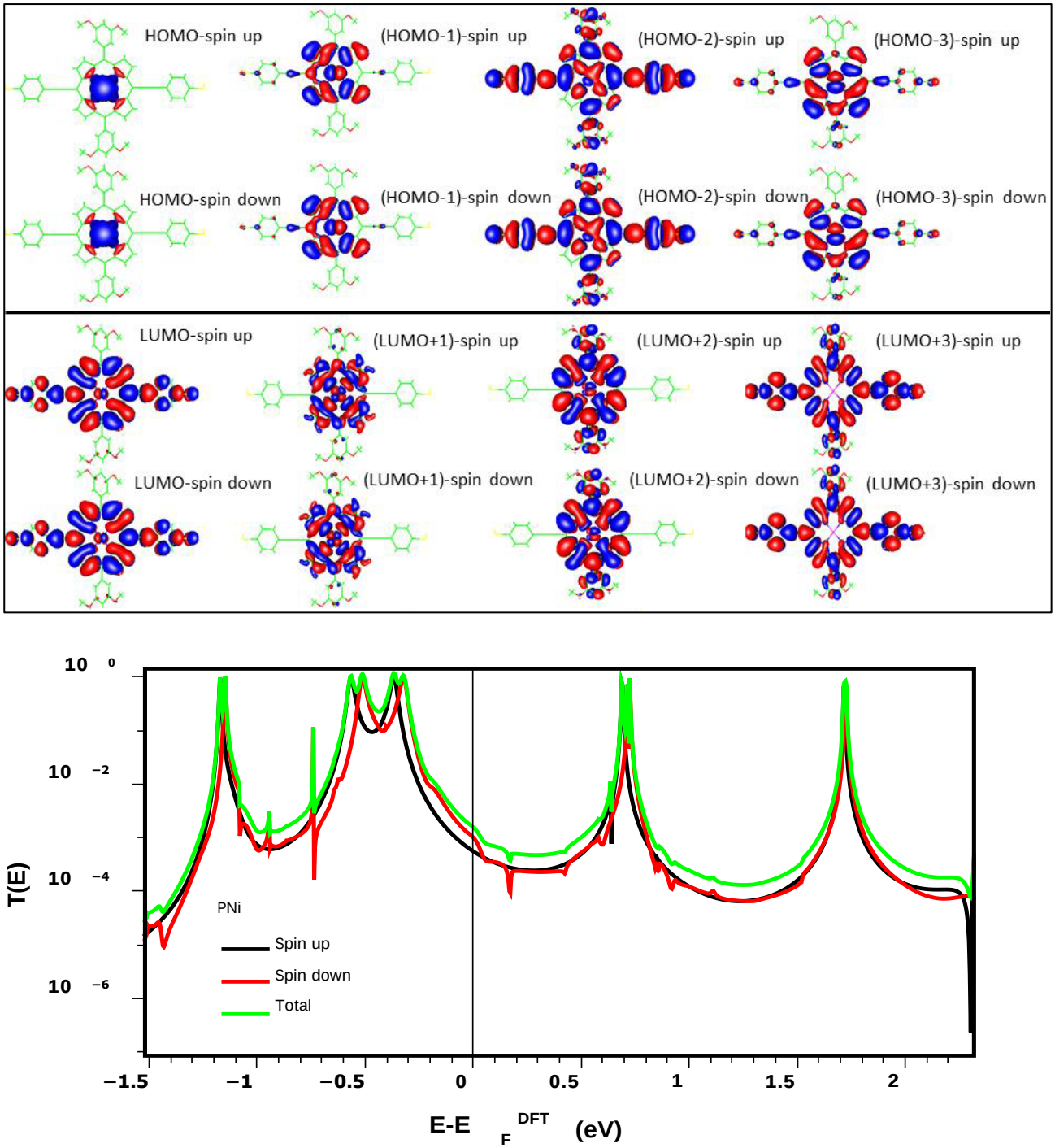

Figure S6: Frontier molecular orbitals of the PNi obtained using the spin- dependent DFT. Red corresponds to positive and blue to negative regions of the wave functions. Below each plot of molecular orbitals, we present the spin-dependent and total transmission coefficients as a function of energy.

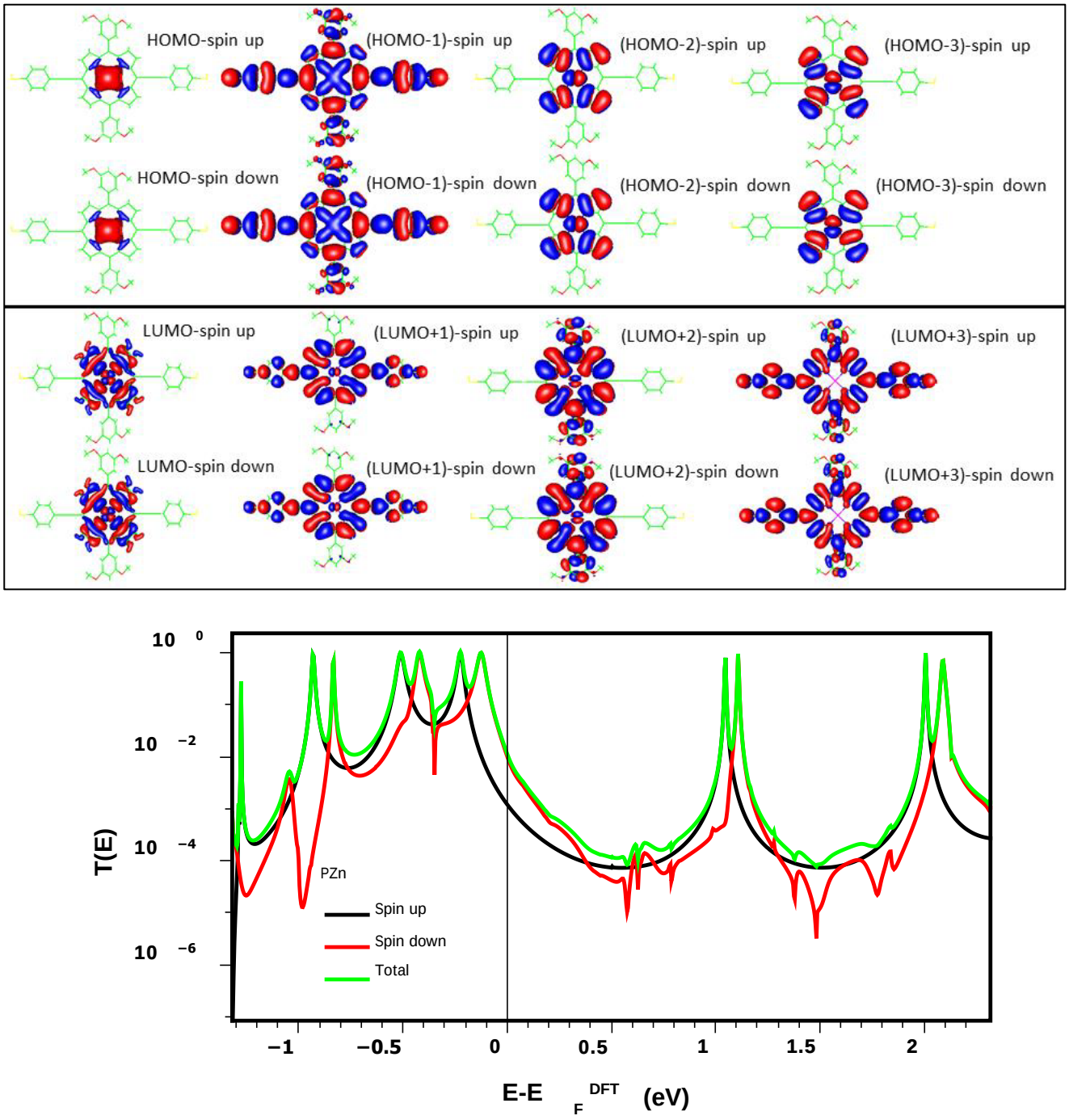

Figure S7: Frontier molecular orbitals of the PZn obtained using the spin- dependent DFT. Red corresponds to positive and blue to negative regions of the wave functions. Below each plot of molecular orbitals, we present the spin-dependent and total transmission coefficients as a function of energy.

Thermoelectric properties of Fe(III)-porphyrin in presence of a Cl counter anion.

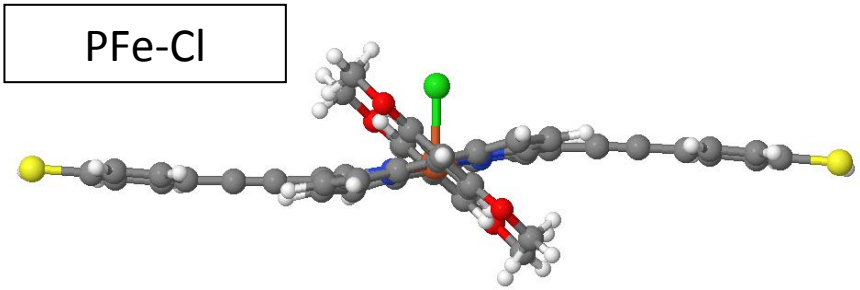

Figure S8: Optimized geometry of porphyrin with central Fe(III)-Cl complex.

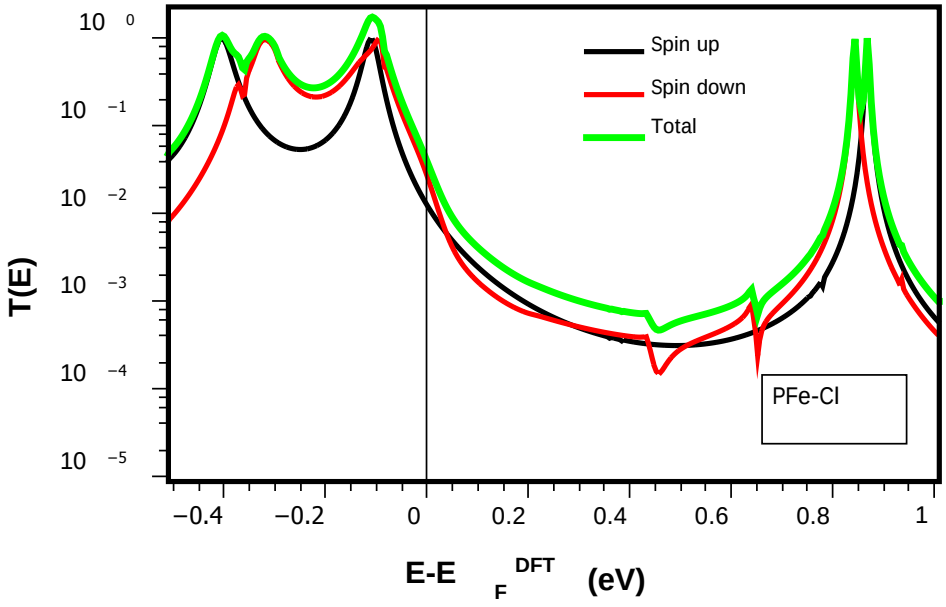

Figure S9: The spin-dependent and total transmission coefficients as a function of energy for Fe(II)-porphyrin in presence of a Cl counter anion, the structure of which is shown in figure S8.

Figure S9 shows spin-dependent and total transmission coefficients relative to the DFT-predicted Fermi energy E_F^{DFT} of the Fe(III)-porphyrin in presence of a Cl^- counter ion. The green line shows that total transport through the Fe-Cl-porphyrin is HOMO-dominated, whereas for the non-complexed Fe(II)-porphyrin (see Figure 3b of main text) transport is LUMO dominated.

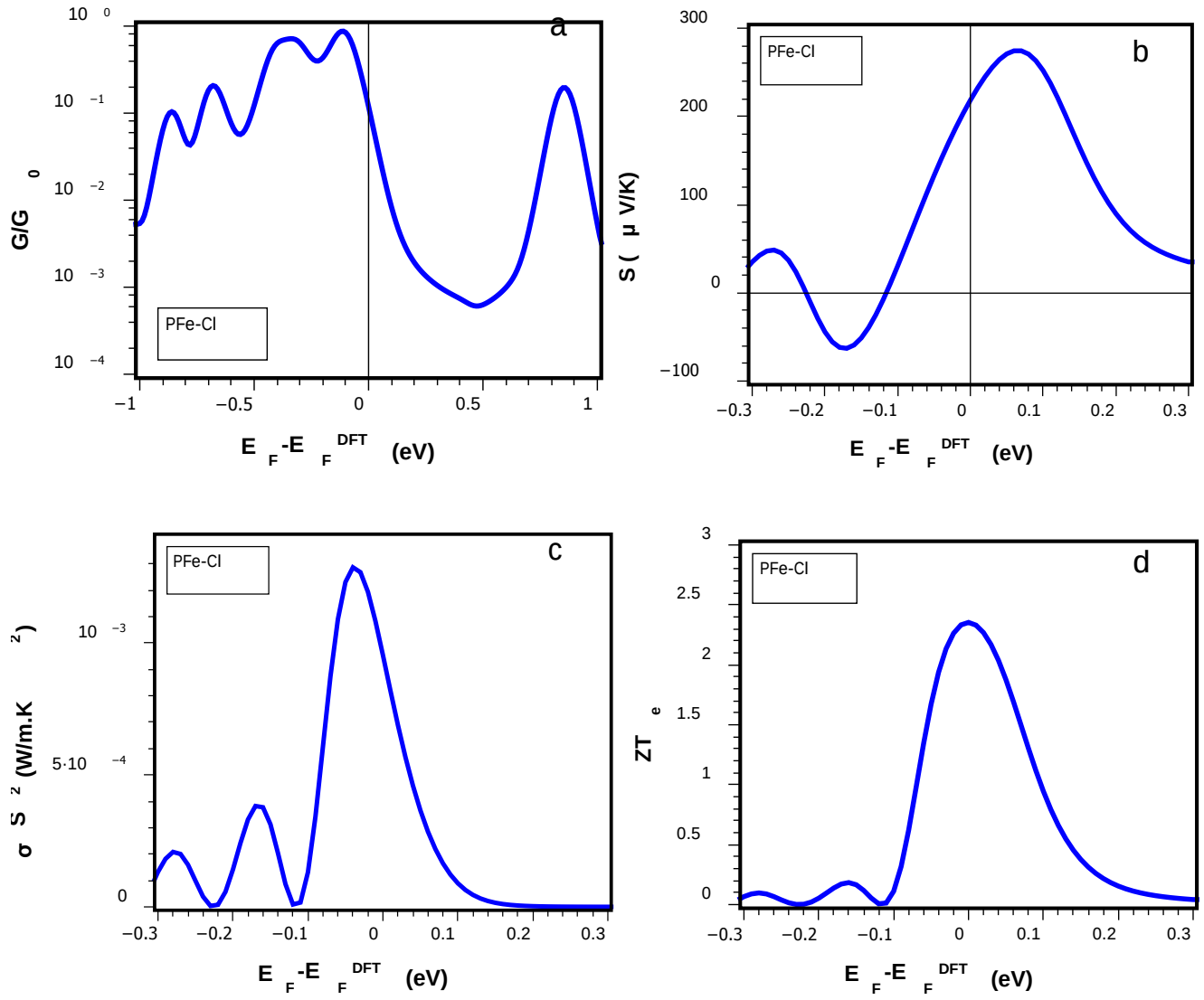

Figure S10. For the structure in figure S8, figures (a, b, c and d) show the room-temperature electrical conductance *G*, thermopower *S*, power factor $P = S^2\sigma$ and electronic figure of merit ZT_e over a range of Fermi energies E_F relative to the DFT-predicted Fermi energy E_F^{DFT}.

Figure S10a shows the room-temperature electrical conductance for Fe-porphryin in presence of Cl^- .shown in Figure S8. The HOMO-dominated conductance at the DFT Fermi energy leads to the positive Seebeck coefficient (thermopower) *S* shown in Figure S10b, the power factor $S^2\sigma$ (Figure S10c) and electronic contribution to the figure of merit ZT_e (Figure S10d), all at room temperature. These results are

for a range of Fermi energies E_F relative to the DFT-predicted Fermi energy E_F^{DFT}. Figure S10b demonstrates that in presence of Fe(III)-Cl at the centre of the porphyrin monomer, the magnitude of thermopower *S* is changed to +218 $\mu V/K$, compared with -260 $\mu V/K$ for Fe(II).

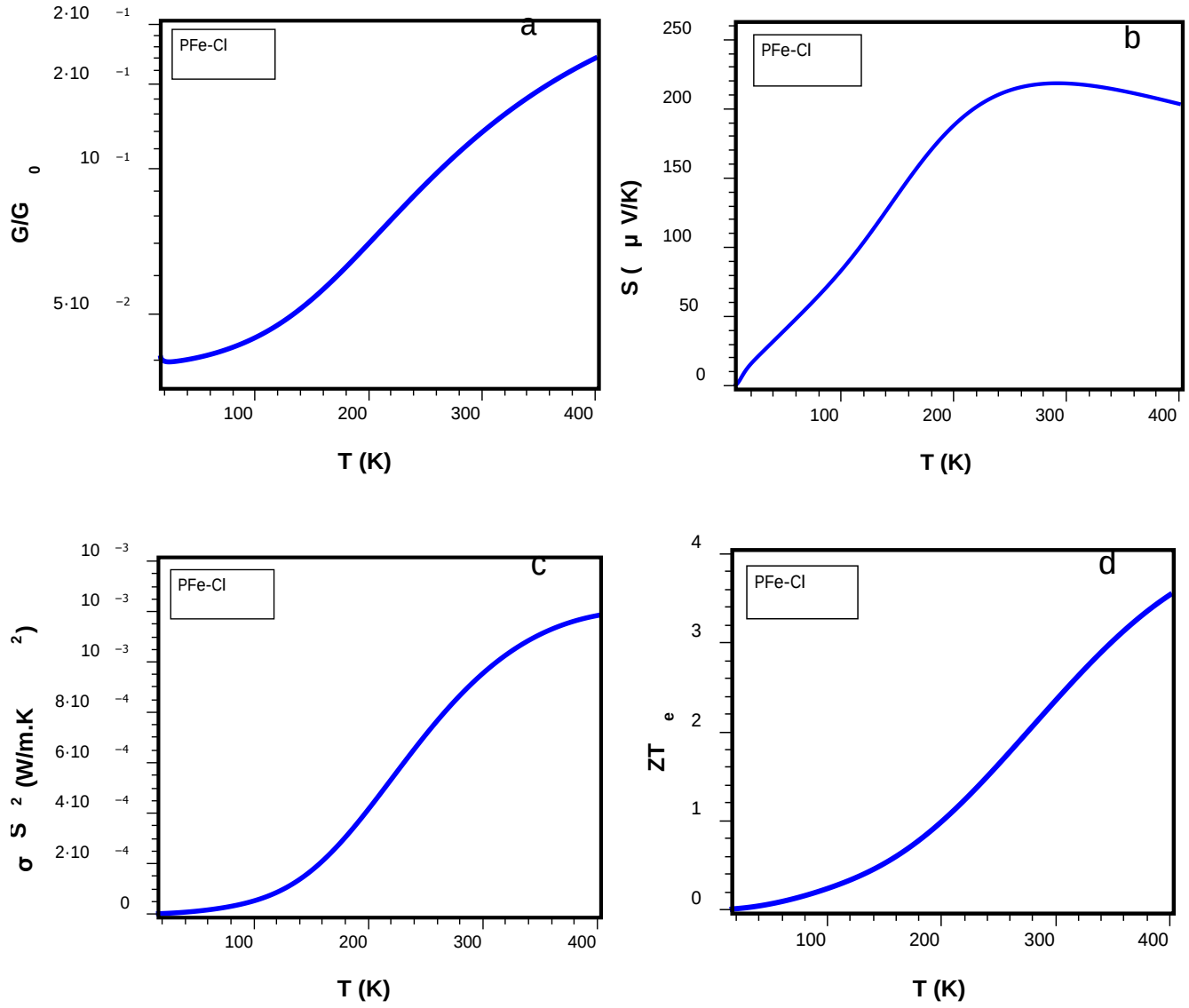

Figure S11: For the structure in figure S8, figures (a, b, c and d) show the electrical conductance, Seebeck coefficients *S* (thermopower), power factor $P = S^2\sigma$, electronic contribution to the figure of merit ZT_e as a function of temperature, evaluated at $E_F = E_F^{DFT}$.

Figure S11 shows the electrical conductance G, Seebeck coefficients *S* (thermopower), power factor $S^2\sigma$ and electronic figure of merit ZT_e as a function of temperature for the structure in figure S8, obtained using the DFT-predicted Fermi energy E_F^{DFT}.

The calculation of Mn-porphyrin in presence of (Cl).

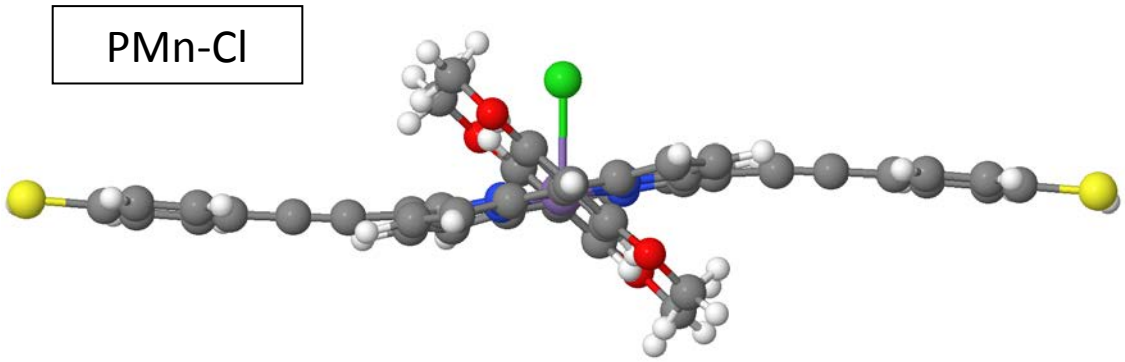

Figure S12: Optimized geometry of porphyrin with central Mn(III)-Cl complex.

For the structure in Figure S12, Figure S13 shows spin-dependent and total transmission coefficients relative to the DFT-predicted Fermi energy E_F^{DFT}. The green line shows that the total transmission through the Mn(III)-Cl porphyrin is HOMO-dominated, whereas Figure 4b of the main text shows that for Mn(II) porphyrin transport is LUMO dominated.

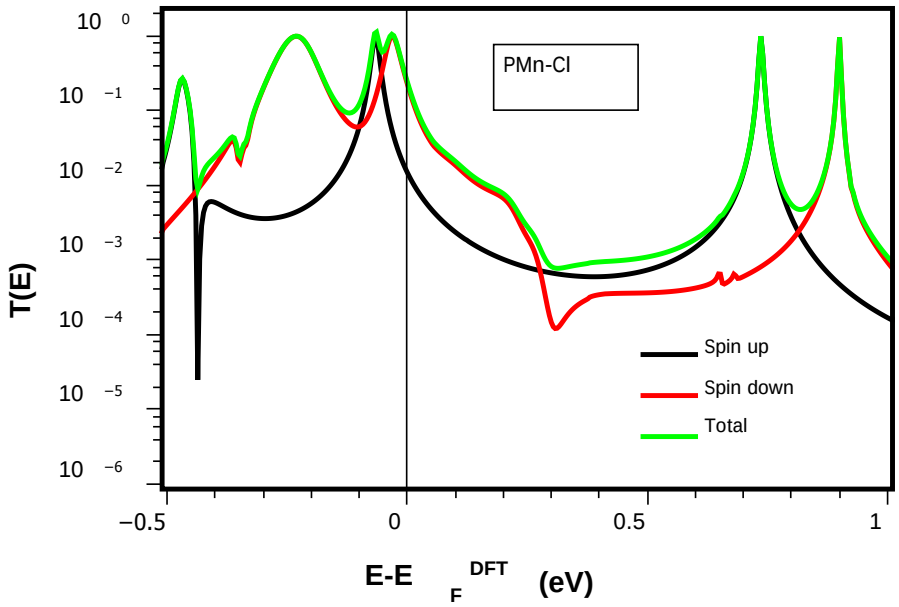

Figure S13: The spin-dependent and total transmission coefficients as a function of energy for Mn-porphyrin in presence of (Cl), which is shown in figure S12.

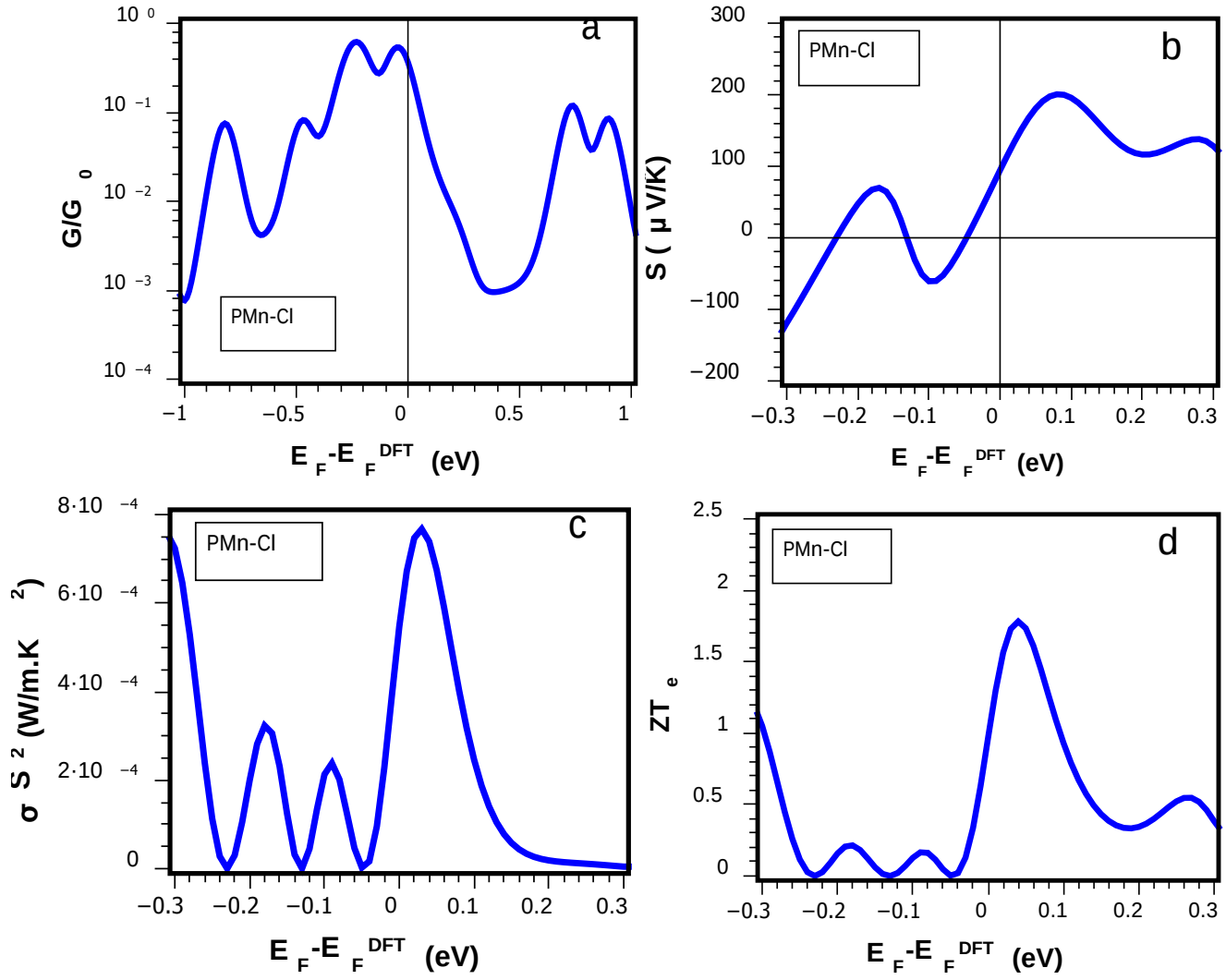

Figure S14. for the structure in figure S12, figures (a, b, c and d) show the room-temperature electrical conductance *G*, thermopower *S*, power factor $P = S^2\sigma$ and electronic figure of merit ZT_e over a range of Fermi energies E_F relative to the DFT-predicted Fermi energy E_F^{DFT}.

For the structure in figure S12, Figure S14 shows that the room-temperature electrical conductance for Mn-porphryin in presence of (Cl^-) is HOMO-dominated conductance at the DFT Fermi energy. Figure S14b, S14c and S14d show results for the Seebeck coefficient (thermopower) *S*, power factor $S^2\sigma$, electronic contribution to the figure of merit ZT_e at room temperature. These results are for a range of Fermi energies E_F relative to the DFT-predicted Fermi energy E_F^{DFT}. Figure S14b demonstrates that in presence of Mn-Cl at the centre of the porphyrin monomer, the magnitude of thermopower *S* is changed to +95 $\mu V/K$.

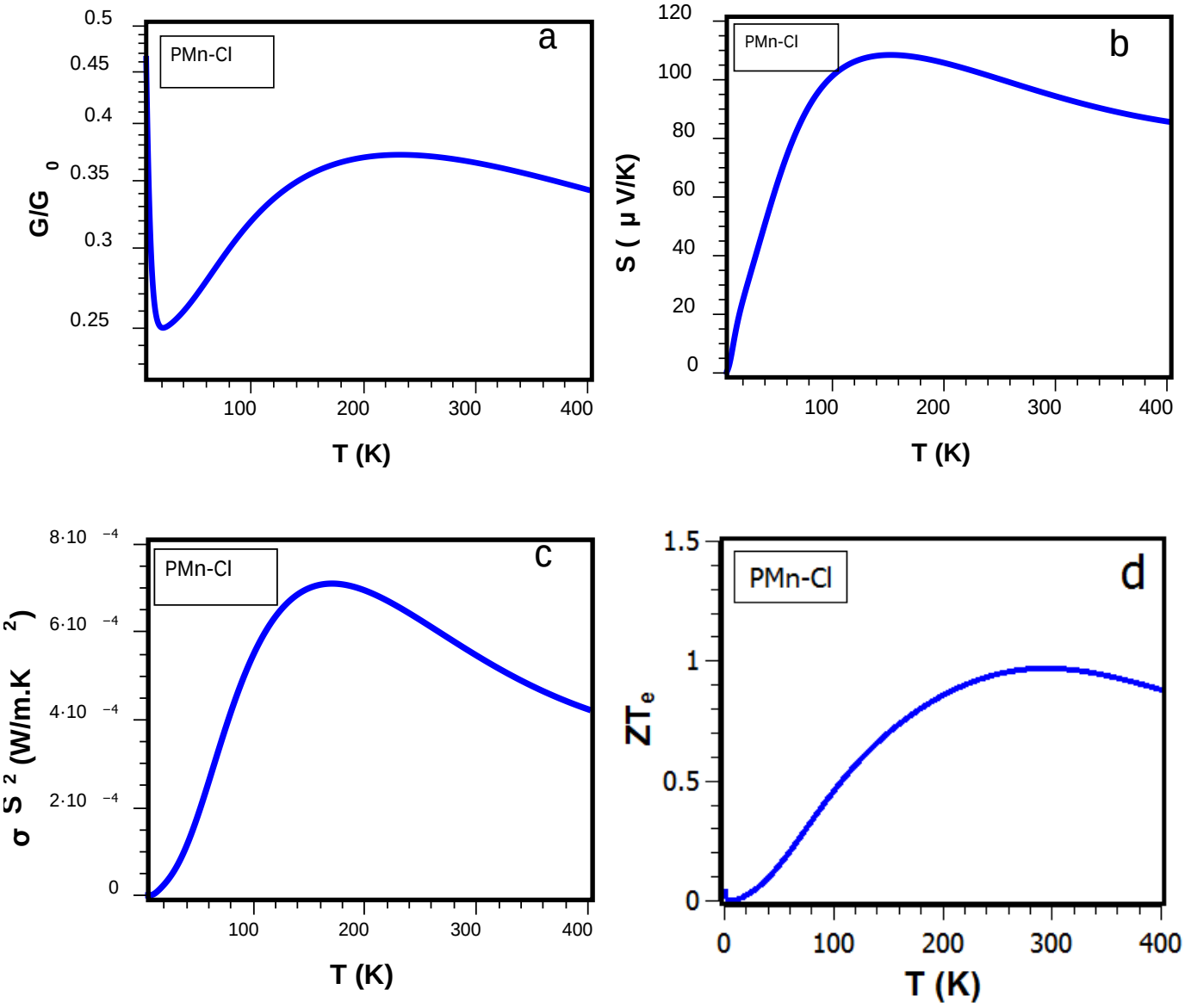

Figure S15: For the structure in figure S12, (a, b, c and d) represent the electrical conductance, Seebeck coefficients *S* (thermopower), power factor $P = S^2\sigma$, electronic contribution to the figure of merit ZT_e as a function of temperature, evaluated at $E_F = E_F^{DFT}$.

For the structure in figure S12, Figures S15(a, b, c and d) show the electrical conductance *G*, Seebeck coefficients *S* (thermopower), power factor $S^2\sigma$ and electronic figure of merit ZT_e as a function of temperature, obtained using the DFT-predicted Fermi energy E_F^{DFT}.